Scalability in Computing and Robotics

Heiko Hamann[1]   Andreagiovanni Reina[2]

[1] Institute of Computer Engineering, University of Lübeck,
Lübeck, Germany
[2] IRIDIA, Université Libre de Bruxelles, Brussels, Belgium;
Department of Computer Science, University of Sheffield,
Sheffield, UK

June 14, 2021

Abstract

Efficient engineered systems require scalability. A scalable system has increasing performance with increasing system size. In an ideal situation, the increase in performance (*e.g.*, speedup) corresponds to the number of units (*e.g.*, processors, robots, users) that are added to the system (*e.g.*, three times the number of processors in a computer would lead to three times faster computations). However, if multiple units work on the same task, then coordination among these units is required. This coordination can introduce overheads with an impact on system performance. The coordination costs can lead to sublinear improvement or even diminishing performance with increasing system size. However, there are also systems that implement efficient coordination and exploit collaboration of units to attain superlinear improvement. Modeling the scalability dynamics is key to understanding and engineering efficient systems. Known laws of scalability, such as Amdahl's law, Gustafson's law, and Gunther's Universal Scalability Law, are minimalistic phenomenological models that explain a rich variety of system behaviors through concise equations. While useful to gain general insights, the phenomenological nature of these models may limit the understanding of the underlying dynamics, as they are detached from first principles that could explain coordination overheads or synergies among units. Through a decentralized system approach, we propose a general model based on generic interactions between units that is able to describe, as specific cases, any general pattern of scalability included by previously reported laws. The proposed general model of scalability has the advantage of being built on first principles, or at least on a microscopic description of interaction between units, and therefore has the potential to contribute to a better understanding of system behavior and scalability. We show that this generic model can be applied to a diverse set of systems, such as parallel supercomputers, robot swarms, or wireless sensor networks, therefore creating a unified view on interdisciplinary design for scalability.

1 Introduction

Many engineered systems can improve their performance by parallelizing the execution of tasks among its constituent units [Kirk and Wen-Mei, 2016, Hamann, 2018b]. Increasing the system size N (number of units) can lead to an improvement in the system performance, that we understand here as mean throughput $X(N)$ (completed sub-tasks per time).[1] A linear speedup of $S_{\mathrm{thruput}}(N) = X(N)/X(1) = N$ is observed when the N-unit system achieves N-times the throughput of the single-unit system ($N = 1$). However, most systems cannot be scaled up arbitrarily because parallelization comes with a number of constraints. Some tasks, for instance, may not allow to be fully parallelized but have a certain fraction σ of necessarily serial operations. In addition, parallel computing requires a certain level of coordination among units that may negatively impact on the overall performance [Archibald and Baer, 1986, Farkas et al., 1995]. In order to design, predict, and control engineered systems, models describing the system's scalability are needed.

We propose a new model for system scalability that has increased explanatory power compared to previously published approaches [Amdahl, 1967, Gustafson, 1988, Gunther, 1993]. First, we abstract the behavior of individual system units to a three-state finite state machine. That state machine also serves as a population model representing percentages of the system's units that stay in each of these three states during a transient and in equilibrium. Second, we link the microscopic level (individual unit behavior) with the macroscopic level (system behavior) as we start from reaction equations of individual behavior and give the respective population model. Third, we derive previous scalability models as special cases of ours. Besides the formulation of the model, our second main contribution is to point to the generality of system scalability behaviors across diverse fields, such as computing, robotics, and networks.

1.1 Laws of scalability

One of the first attempts of modeling such system behavior came from Amdahl [Amdahl, 1967] who was motivated by empirical evidence and aimed to highlight the limitations of parallel computing. While the actual equation was not provided in the initial publication, Amdahl's law was later formalized as a function describing the speedup $S_{\mathrm{thruput}}(N) = X(N)/X(1)$. Amdahl's law reads as

$$S_{\mathrm{thruput}}(N) = \frac{N}{1 + \sigma(N - 1)} \ , \tag{1}$$

where $0 \leq \sigma \leq 1$ is the amount of time spent on serial parts of the task. As illustrated in Fig. 1a, Amdahl's law predicts a bounded scalability of performance, that is, $S_{\mathrm{thruput}}(N)$ saturates at an approximately constant value of σ^{-1} for any large N.

---

[1]Alternatively, one can define speedup based on latencies: $S = T(1)/T(N)$ with $T(1)$ is the time one has to wait until the single-unit system is done and $T(N)$ is the time of the N-unit system.
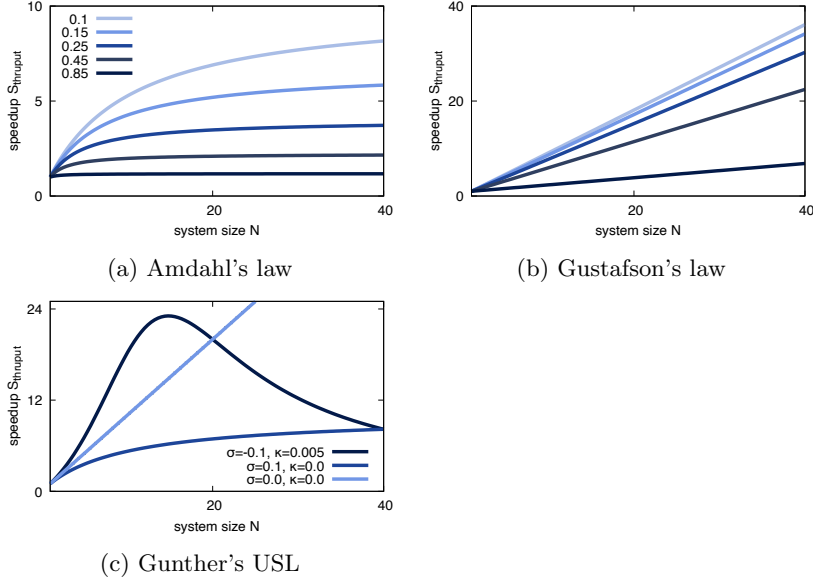
(a) Amdahl's law

(b) Gustafson's law

(c) Gunther's USL

Figure 1: Speedup S_{thruput} as a function of the system size N (*e.g.*, number of processors, robots, users) according to three known laws of scalability. (a) Amdahl's law (Eq. 1) for serial proportion parameter $\sigma \in \{0.1, 0.15, 0.25, 0.45, 0.85\}$ shows performance increase for small N and saturation to a constant performance for large N. (b) Gustafson's law (Eq. 2) shows a unbounded increase of performance with increasing system size. (c) Gunther's Universal Scalability Law (USL, Eq. (3)) can show a richer set of dynamics including diminishing returns (for positive coherence delay $\kappa > 0$) and superlinear speedups (for negative contention $\sigma < 0$); the USL curves in panel (c) is for $\sigma = 0$ and $\kappa = 0$, $\sigma = 0.1$ and $\kappa = 0$, $\sigma = -0.1$ and $\kappa = 0.005$

Later, a more optimistic perspective was provided by Gustafson's law [Gustafson, 1988]

$$S_{\text{thruput}}(N) = N + (1 - N)\sigma \; , \tag{2}$$

which assumes that the impact of the serial part $0 \leq \sigma \leq 1$ on the speedup $S_{\text{thruput}}(N)$ decreases with system size N. Therefore, Eq. (2) leads to an unbounded growth of $S_{\text{thruput}}(N)$ by increasing N as shown in Fig. 1b.

Later, Gunther [Gunther, 1993] drew attention to the possibility that for large systems, coordination overheads for increased system size may be larger than the work that can be done by the added units. The performance of a system with a size larger than critical value N_c retrogrades by increasing N. Operating a system with size $N > N_c$ is outright undesirable due to the combined cost of additional units and reduced overall performance. Instead, it is particularly useful to have models that can predict the value of N_c and help to avoid operating systems in the region $N > N_c$. Gunther [Gunther, 1993] extended Amdahl's law to define the Universal Scalability Law (USL) as

$$S_{\text{thruput}}(N) = \frac{N}{1 + \sigma(N - 1) + \kappa N(N - 1)} \; , \tag{3}$$

where σ is now called contention (time lost queuing for shared resources) and the additional parameter κ accounts for the coherency delay (overheads of coordinating many units).[2] The underlying idea is that a cost proportional to the square of the system size $\propto N^2$ is necessary to administrate the system. A quadratic increase in the coordination cost corresponds to the assumption of a coherency delay κ caused by the interaction of every unit with all other $N - 1$ units (all-to-all interaction or a constant fraction of all-to-all interaction resulting in $\mathcal{O}(N^2)$ overhead). This type of problem is frequent in parallel programs with shared memory that need to ensure cache coherency, for example, by employing protocols, such as bus snooping [Archibald and Baer, 1986, Farkas et al., 1995]. Note that setting $\kappa = 0$ in Eq. (3) is Amdahl's law (Eq. (1)). Setting $\sigma = 0$ and $\kappa = 0$ models a linear speedup $S_{\text{thruput}}(N) = N$ similar to Gustafson's law. Despite scalability analysis in the region $N > N_c$ has been largely ignored by others than Gunther, we argue that knowledge about the system performance in the full system size domain, including $N > N_c$, can give a better understanding of the system behavior.

1.2 Retrograde performance and superlinear speedups

Retrograding performance can be observed in models in which increasing the system size triggers a nonlinear slowdown. Therefore, once going beyond the critical size N_c, the added benefits of additional units are smaller than the caused slowdown, for example, due to required access to shared resources. In queuing

---

[2]Note that there is an unpublished 3-parameter USL model variant by Gunther where a third parameter γ is multiplied to eq. 3. It is equivalent to a Gustafson factor and can represent the throughput for $N = 1$.

theory, the *repairman* model [Allen, 1990] is a simple classical model that describes how a shared resource can limit the system's throughput. In this model, the shared resource is the repairman who can only repair machines sequentially, taking time S per machine. The model assumes that machines periodically need downtime (repair time) and shows that for large number of machines N the system throughput saturates to $1/S$ [Gunther, 2007], reproducing the behavior of Amdahl's law. Throughput saturation is caused by each machine getting periodically unproductive for the repair time R that sums both the repairman's service time S and waiting time W. However, to model retrograde performance, the repair time R needs to nonlinearly increase with increasing waiting time W due to longer queues. Gunther [Gunther, 2008] indicated that assuming a quadratic increase of R, the repairman model becomes the state-dependent server model $M/G/1//p$ from queuing theory [Gittins et al., 1989]. From this state-dependent model, Gunther [Gunther, 2008] was able to derive a specific form of the USL ($\kappa = c\sigma$ for a constant $c > 0$) where the term $N(N-1)$ in Eq. 3 directly follows from nonlinearly increasing repair times $R \propto N(N-1)$. In this way, he got close to a scalability law based on first principles but the state-dependent server model already contains the nonlinear repair times as a modeling assumption. Hence, also this approach has limited potential for insights into the underlying system behavior.

Gunther's USL also covers another crucial, and at the same time controversial, phenomenon of parallel computing: superlinear speedup, that is, $S_{\text{thruput}} > N$. Naively, one may assume that linear speedup of $S_{\text{thruput}} = N$ is the ideal case. However, Gunther et al. [Gunther et al., 2015a] have shown that superlinear speedups occur in actual computing systems, such as in systems for distributed storage and processing of big data (*e.g.*, Apache Hadoop [ASF - Apache Software Foundation]). These surprising results question the initial doubts about whether superlinear speedups can exist [Gustafson, 1990, Helmbold and McDowell, 1990]. In parallel computing, a common criticism to superlinear speedups has been that a single-processor machine could, in theory, emulate any N-processor machine to achieve the same speedup performance. Hence, superlinear speedup has been claimed to only take place on suboptimal sequential algorithms [Grama et al., 2003]. Such a point of view, however, ignores physical constraints that could render such an emulation impossible, such as cache effects or synergistic collaboration between processors.

Scalability analysis studies the performance for increasing system size, that is, for adding units. A unit needs to have potential to positively contribute to system throughput. Since throughput is defined as completed sub-tasks per time, it can be scaled in two dimensions: provided work force and provided sub-tasks. A system can be limited in two ways: shortage in workers and/or shortage in sub-tasks. A unit's contribution, hence, can be of two kinds: adding work force and/or adding sub-tasks. An added robot in a multi-robot system increases work force and an added user in a database benchmark increases system load. In both cases, the unit adds to the overall demand on shared resources. The robot requires a section of shared space to navigate and the user requires computation time on the shared processor. It is important to understand that

depending on how we define the units, we can obtain different scalability outcomes. We can assume *pure* units that add resources in only a single dimension, for example, only a computation module, or only a memory module. Differently, we can assume *combined* units that add a set of resources, for example, in parallel computing an added CPU may also include some memory (such as CPU cache), or in robotics an added robot includes computation, memory, sensing, and actuation resources. We believe that pure units are better fitted to theoretical analysis, while combined units are closer to what is observed in real systems. In parallel computing, adding computing power without any memory may be unfeasible as CPU cache is integrated in microprocessors. Even more so in robotics, adding pure units for computation, for example, would require redesigning the robots to maintain the memory, sensing, and actuation of the group constant while increasing the computation only. In relation to the discussion of superlinearity [Gustafson, 1990, Helmbold and McDowell, 1990, Grama et al., 2003, Gunther et al., 2015a,b], we believe that the possibility and impossibility of superlinear speedups is linked to the distinction between pure and combined units as yet overlooked. Superlinear speedup is not theoretically possible with pure units, while it can be observed, both in computing [Gunther et al., 2015a,b] and in robotics [Ijspeert et al., 2001, O'Grady et al., 2007, Talamali et al., 2020], considering combined units. In computing, superlinear speedups are a consequence of the combination of increased computing power and cache, in what is a so-called *cache effect* [Gunther et al., 2015a]. Through cache effects, the combined cache of all N CPUs reaches a size large enough to allow the execution of the entire task on each CPU without access to external memory. In multi-robot systems, superlinear speedups are also caused by a combination of added resources. For example, O'Grady et al. [O'Grady et al., 2007] showed that a team of $N = 3$ physically connected robots can cross a gap that cannot otherwise be bridged by a single robot. In this case, the robots physically connect with each other and hence benefit from a combination of more traction power and a larger base area. Note that, to observe a superlinear speedup, the workload must be kept constant. If the workload would be increased with the number of CPUs, the cache effect would not be observed. Similarly, if the gap would be made wider for increased robot team size, no team could cross it.

In order to allow the USL to describe superlinear speedups, parameter σ must be negative (see Fig. 1c). Therefore, the initial interpretation of parameter σ as the serial fraction of the task was changed to interpret it as contention. Positive contention (*i.e.*, $\sigma > 0$) describes the overhead cost due to coordination of shared resources while negative contention (*i.e.*, $\sigma < 0$) describes the effects of synergistic interaction among the units, for instance collaborating robots.

1.3 Scalability in multi-robot systems

In multi-robot systems, similar performance curves have been observed and scalability is a key aspect of numerous studies [Hamann, 2018b, Bjerknes and Winfield, 2013, Talamali et al., 2020]. Hamann [Hamann, 2018a] followed a mostly phenomenological approach by fitting performance curves from the swarm robotics

literature. The adopted function to model the swarm performance is

$$S_{\text{thruput}}(N) = aN^b \exp(cN) \ , \tag{4}$$

for constants $a > 0$, $b > 0$, and $c < 0$. The function can be understood as a dichotomous pair of a term for potential of collaboration N^b and a term for interference $\exp(cN)$. This model was fitted to a number of application scenarios in swarm robotics, such as foraging, collective decision-making, and collective motion [Hamann, 2013, 2018a] and it bears similarity to models of the slotted ALOHA communication protocol [Roberts, 1975, Gokturk et al., 2008]. While the speedup and performance curves in computing and multi-robot systems can be similar, a key difference is that certain multi-robot applications require the collaboration of robots. For these cases, the task cannot be solved unless two or more robots interact and work together. Examples are the stick pulling scenario [Ijspeert et al., 2001] and the the emergent taxis scenario [Bjerknes et al., 2007]. In stick pulling, two robots are required to pull a stick due to mechanical constraints. In emergent taxis, robots collectively move towards a beacon while an individual robot would not be able to do so due to limited sensors.

1.4   Related efforts in other disciplines

Our ultimate goal of finding a generic function of performance over system size relates to several efforts in other fields, such as network theory and statistical physics. For example, Feng et al. [Feng et al., 2020] study how the Pareto distribution and the log-normal distribution can be used to fit degree distributions of scale-free networks. Similarly to this paper they also validate their approach empirically by fitting their model to data from applications. Note that we focus on functions of speedup over system size but we speculate that the underlying interaction networks (*e.g.*, defined by required coordination of processors or mutual perception of robots) also scale and probably change their node degree distributions significantly [Khaluf et al., 2017, Bettstetter, 2004]. The study by Lazer and Friedman [Lazer and Friedman, 2007] is an example where group performance is directly related to network topology.

As we try to model interacting computers, robots, and other agents, there are many related fields that have studied similar systems. Often a formalism borrowed from statistical physics and chemical kinetics, such as rate equations and other ODE systems, are applied [Espenson, 1995]. Rate equations have been used extensively in parallel computing and networks to model stochastic communication, for example, rumor or virus spreading (gossiping) [Dumitras and Marculescu, 2003, Zhang et al., 2007, Bogdan and Marculescu, 2009, Sayama et al., 2013].

1.5   Scalability across disciplines

Models describing the scalability of parallel computers or robot swarms have been instrumental to gain important insights about the system dynamics, how-

ever they are limited by one common aspect. The models are phenomenological in the sense that they have been derived to effectively match the observed throughput S_{thruput} without explaining how the system *behaves* and therefore why the performance varies. We contribute towards this endeavor by employing our expertise in decentralized system theory [Resnick, 1994, Martinoli et al., 2004, Garnier et al., 2007, Hamann, 2018b] to formalize a general model that unifies scalability dynamics of a diversity of systems, from parallel computers to robot swarms. The proposed model is based on generic rules that describe interactions between units and how these interactions change the state of the units and, in turn, of the whole system. Therefore, the scalability dynamics of our model are the results of a mechanistic explanation of the system. Such a bottom-up description paradigm is, for example, core in the emerging field of *machine behavior* [Rahwan et al., 2019]. Our results contribute towards the endeavor to engineer and control machine interactions based on a deep understanding of their behavior. Thanks to its generality, our model is of potential interest to both the distributed robotics and the parallel computing communities, as it can flexibly describe the dynamics of a variety of systems and help in the understanding of their causes. While we do not discuss it here, we envision sensor networks, transport systems, chemical systems, and collective animal behavior to be potential further fields of application.

2 Model

Following decentralized system theory, we describe a parallel system as composed by a number N of interacting units (*e.g.*, processors, robots, users) that work towards the same task. A unit at each moment can be in one of three possible states: *solo* (S), *grupo* (G), and *fermo* (F).[3] These states indicate how the unit is working toward completing the task (see state machine in Fig. 2). A unit can be either working in solitary mode (S), interacting with other units (G), or being unproductive due to congestion on shared resources (F). Depending on the task and the application, units in each of these states can contribute in varying degrees to the system performance (as later indicated by Eq. (15)).

2.1 Transition rates

The model describes changes in a unit's state via transition rates which determine the conditions and speed of such changes. The state transitions can be described via reaction stoichiometry in the form of balanced equations:

$$2S \xrightarrow{k_1} 2G \tag{5}$$

$$S + G \xrightarrow{k_2} 2G \tag{6}$$

$$S + F \xrightarrow{k_3} G + F \tag{7}$$

---
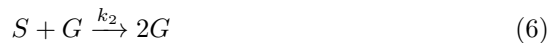
[3]These words are loosely adapted from Esperanto and Italian: sole/solo for alone, grupo/gruppo for group, fermo/fermo for stationary or firmly.
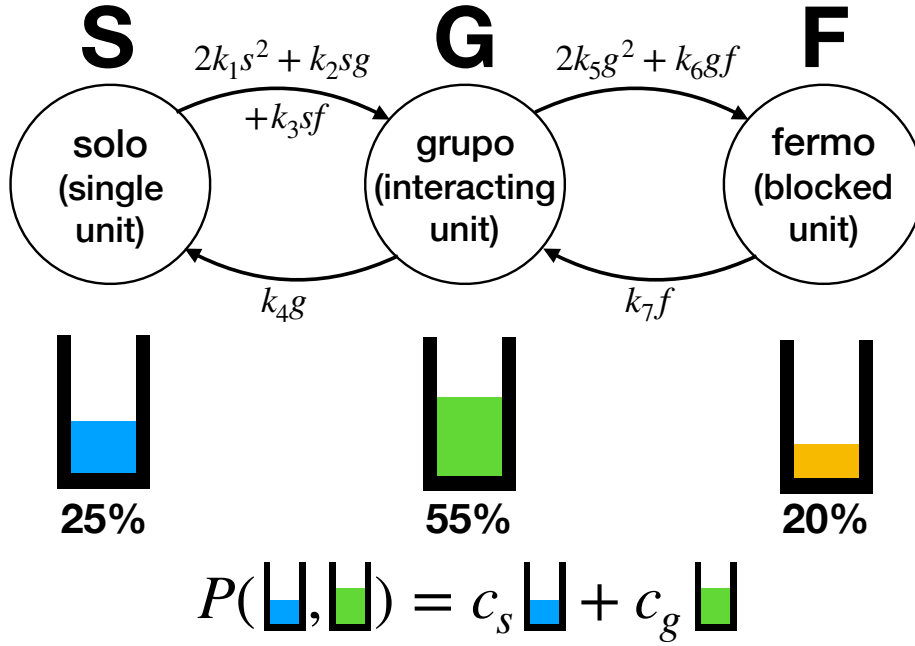
8

Figure 2: Graphical representation of the proposed model in the form of a three-state machine: solo units (state S), interacting units (state G), and blocked units (state F). The number of units is constant (Eq. (13)) and they change their state (arrows) according to the model of Eqs. (5)-(11). As indicated in Eq. (15), the number of units in each state determines the system performance.

$$G \xrightarrow{k_4} S \tag{8}$$

$$2G \xrightarrow{k_5} 2F \tag{9}$$

$$G + F \xrightarrow{k_6} 2F \tag{10}$$

$$F \xrightarrow{k_7} G . \tag{11}$$

The seven transitions with respective rates k_i (with $i \in \{1, 2, \ldots, 7\}$) determine the system dynamics and can be interpreted as follows. The transitions of Eqs. (5)-(7) describe individual units (state *solo S*) that begin an interaction with other units and change their state to *grupo G*. The transitions of Eqs. (9) and (10) describe interacting individuals (state *grupo G*) that due to congestion on a shared resource go to blocked state *fermo F*. Finally, Eqs. (8) and (11) respectively describe units completing their interactions and decongesting. Note that units do not directly change state from *solo S* to *fermo F* nor viceversa. Instead, in order to reach or decongest a *fermo* state, units always go through an interaction with other units via state *grupo G* to model cost paid in time due to switching overheads.

The seven transition rates k_i determine the frequency of transitions as single unit actions (*i.e.*, Eqs. (8) and (11)) or, in other cases, conditional to contact between two units in specific states (*i.e.*, Eqs. (5)-(7), (9) and (10)). By modulating the relative frequency of the seven transition rates k_i, the model can describe any previously observed scalability law and establish a link between the units' state change and the whole system performance, as illustrated in Sec. 3.

2.2 Mathematical model

Through van Kampen expansion [van Kampen, 1981], the model of Eqs. (5)-(11) can be written in the form of a system of ordinary differential equations (ODEs):

$$\begin{cases} \dfrac{ds}{dt} = -2k_1 s^2 - k_2 sg - k_3 sf + k_4 g \\[2mm] \dfrac{dg}{dt} = 2k_1 s^2 + k_2 sg + k_3 sf - k_4 g - 2k_5 g^2 - k_6 gf + k_7 f \\[2mm] \dfrac{df}{dt} = 2k_5 g^2 + k_6 gf - k_7 f , \end{cases} \tag{12}$$

where the system variables s, g, and f represent the number of units in states *solo S*, *grupo G*, and *fermo F*, respectively. The model of Eq. (12) is a macroscopic description of the system as it describes how the population of units is divided between three subpopulations in distinct states and how these subpopulations change over time. The proposed model is a closed system that describes a population comprised of a constant number of units with dynamic states. We can therefore replace one of the differential equations of Eq. (12) with the equation

$$N = s + g + f , \tag{13}$$

obtaining a two-equation system (see details in the Appendix). Through stability analysis, we can compute the fixed points of the system of Eq. (12). Among these fixed points, we are interested in studying the stable point (s^*, g^*, f^*) that exists in the positive simplex, that is, the three subpopulations are positive (≥ 0) and smaller than N (see details in the Appendix). Such a stable fixed point can be interpreted as the final state toward which the system asymptotically converges, that is,

$$s^* = \lim_{t \to \infty} s(t) \,, \ g^* = \lim_{t \to \infty} g(t) \,, \ f^* = \lim_{t \to \infty} f(t) \,, \tag{14}$$

for the starting point $s(0) = N, g(0) = 0, f(0) = 0$. Studying how the stable fixed point (s^*, g^*, f^*) changes as a function of the system size N (and transition rates) provides information on the system's scalability. The technical details about the stability analysis are provided in the Appendix.

Note that we derived the ODE system of Eq. (12) borrowing the methodology from statistical physics and chemical kinetics [van Kampen, 1981], which relies on two main assumptions: the system is well mixed and sufficiently large. In a well-mixed system, interactions between any pair of units are equally probable independent of space (cf. law of mass action). The dynamics of systems that have an interaction network far from a well-mixed state could be accurately modeled through more complex models that explicitly include information about the interaction network structure, $e.g.$, by addressing node degrees and neighborhood sizes [Shang and Bouffanais, 2014, Khaluf et al., 2017]. The second assumption is that the system is sufficiently large to ignore the effect of finite-size fluctuations. This assumption could also be relaxed through more complex models, for instance by formulating a master equation—a macroscopic model that explicitly takes into account stochastic fluctuations with magnitudes proportional to system size [Gillespie et al., 2013]—that has already been successfully employed to model multi-core systems [Bogdan and Marculescu, 2011]. The master equation approach was also applied, for example, to multi-agent systems [Lerman and Galstyan, 2001] and traffic flow [Mahnke and Kaupužs, 1999].

2.3   Estimating the performance

The ODE system of Eq. (12) and its fixed points, Eq. (14), indicate how the units of the system divide into the different work states S, G, and F. Depending on their work state, the units contribute differently to the task execution. In our analyses, we assume that units contribute linearly with a tuneable coefficient because nonlinear effects may be incorporated in Eq. (12). However, other contribution functions can be tailored to the performance returns of the specific application scenario. To model the system's performance in terms of throughput X, we define a function that sums the contribution of the units in each state as

$$X(N) = X(s^*, g^*, f^*) = X(s^*, g^*) = c_s s^* + c_g g^* \,, \tag{15}$$

where the contribution coefficients c_s and c_g indicate the contributions to the task execution by units in the two states S and G, and (s^*, g^*, f^*) is the stable fixed point. We assume that units in state *fermo* F do not contribute to task completion because they are in congestion or lack coherency. The system's speedup can be computed as

$$S_{\text{thruput}}(N) = \frac{X(N)}{X(1)} = \frac{X(s^*, g^*, f^*)}{X(1, 0, 0)} = \frac{c_s s^* + c_g g^*}{c_s}$$
$$= s^* + \frac{c_g}{c_s} g^* , \tag{16}$$

for $c_s \neq 0$. The game changer is whether $\frac{c_g}{c_s}$ is greater or smaller than one. If $\frac{c_g}{c_s} > 1$, collaboration is advantageous and one prefers to have units in state G. Otherwise one would prefer units in state S. The contribution coefficients can also be zero as, for example, depending on the task, units in state *grupo* may not contribute to task completion. For $c_g = 0$ we have the standard parallelization problem where we want to keep interactions between units minimal because units in state G do not contribute to task completion. The special case $c_s = 0$ can be understood by studying $\lim_{c_s \to 0} S_{\text{thruput}}(N)$ that results in an infinite improvement of throughput: $S_{\text{thruput}}(N) \to \infty$ for $c_g > 0$, $g^* > 0$, and $c_s \to 0$. Imagine a task that cannot be solved by one robot (*solo* unit) but by two collaborating robots (*grupo* units). We would get $X(1) = 0$ and $X(2) = 1$, hence, an infinite speedup. Fig. 2 shows a graphical representation of how the proportion of units in each state is used to compute the system throughput $X(s^*, g^*, f^*)$. To model systems that benefit from naive parallelization, it is sufficient to set the contribution coefficients to $c_s > 0$ and $c_g = 0$. In such a contribution scheme, only *solo* workers contribute to task completion. This scheme applies to parallel computing in which, typically, the ideal case corresponds to having all the processors operating independently with minimal interaction and hence minimal communication costs [Grama et al., 2003, Ballard et al., 2011]. Consequently, the best performance is attained by limiting interaction and keeping as many processors as possible in the state *solo* S. However, interactions cannot always be avoided and, in certain cases, especially in robotics, exploiting interaction between units can be advantageous, or even essential, to the task completion. Examples of tasks, studied in the literature, that require collaboration in order to be completed are collective transport [Berman et al., 2011] and collective manipulation [Ijspeert et al., 2001] of bulky objects, and self-assembly of robots to cross difficult terrain [O'Grady et al., 2007]. The performance function for tasks that benefit from interaction has the contribution coefficient $c_g > 0$. Therefore, the ratio c_g/c_s determines which state is more productive.

2.4 System size and density

The system size N represents the amount of units (*e.g.*, processors, robots, users) comprising the system. In multi-robot systems, the robots operate in a physical space in which physical interference (*e.g.* collisions) typically plays a

determining role in the task execution and may have an impact on the performance. As one could expect, physical interference is determined by both the number of robots N and the size of the working space A. Therefore, to study the scalability of multi-robot systems, it is appropriate to also consider the impact of the system density $\rho = N/A$, in addition of the system size [Hamann, 2018b]. In this study, we assume a constant working space area $A = 1$ which allows us to appreciate the effect of both density and system size by only varying N.

3 Scenarios

In scalability analysis, three regimes have been identified and described through Gunther's Universal Scalability Law [Gunther, 1993]:

1. ideal concurrency, also described by Gustafson's law (Fig. 1b)

2. contention-limited, that corresponds to Amdahl's law (Fig. 1a)

3. diminishing returns, for example as seen in Fig. 1c.

In the following we discuss these three scalability regimes and show that, through specific parameterizations, our general model can describe all of them. Additionally, our model has the added benefit of establishing a causal link between the scalability regime of the system and the microscopic behavior of its units. In the following representative scenarios, we can obtain the three different regimes by varying the transition rates k_i, while keeping constant the contribution coefficients to $c_s = 1$ and $c_g = 0$, $i.e.$ only $solo$ units (in state S) contribute to the execution of the task. Similar results can be obtained with different contribution coefficients. Additionally, in Sec. 3.4 we show that superlinear increase can be described by parameterizing contribution coefficients to values larger than one. Finally, without loss of generality, we assume that the system is initialized at time $t = 0$ with only $solo$ units, $i.e.$ $s(0) = N, g(0) = 0, f(0) = 0$.
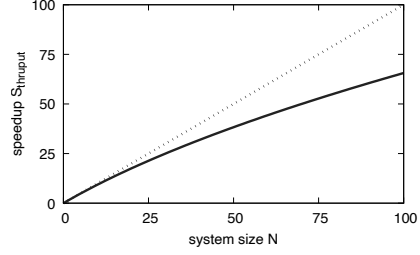
3.1 Ideal concurrency – Gustafson's law

Ideal concurrency, as described by Gustafson's law (Eq. (2)), corresponds to the scenario in which increasing the system size leads to unbounded increase in performance. The optimal case consists in a linear increase of the performance as $S_{\text{thruput}} = N$. A situation where units do not interact and hence act independently from each other. In Gustafson's law of Eq. (2), this situation is obtained by setting the serial proportion parameter $\sigma = 0$, and similarly, in Gunther's USL of Eq. (3) by setting both the contention and coherency delay parameters $\sigma = \kappa = 0$. In our model, the lack of any interaction can be parameterized by setting all the transition rates to zero ($k_i = 0$ for $i \in \{1, 2, \ldots, 7\}$). In this case, the stable point is $(s^* = N, g^* = 0, f^* = 0)$ and thus $P(s^*, i^*, j^*) = N$.
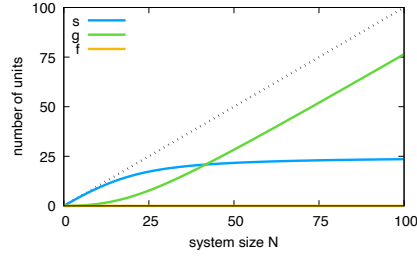In Gustafson's law of Eq. (2), when the serial proportion parameter $\sigma > 0$, the system performance keeps increasing with N, however at sublinear speed. Our model can describe this scenario by setting the rates $k_1 > 0$ and $k_4 > 0$, while
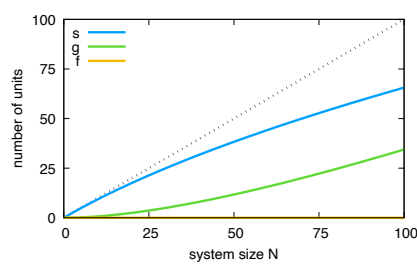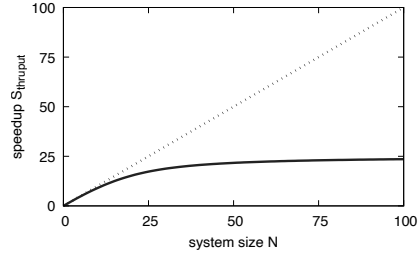
(a) ideal concurrency (Gustafson's law), states of units ($k_1 = 0.004$, $k_4 = 1.0$)

(b) ideal concurrency (Gustafson's law), speedup ($k_1 = 0.004$, $k_4 = 1.0$, $c_s = 1$, $c_g = 0$)

(c) contention-limited (Amdahl's law), states of units ($k_1 = 0.004$, $k_2 = 0.04$, $k_4 = 1.0$)

(d) contention-limited (Amdahl's law), speedup ($k_1 = 0.004$, $k_2 = 0.04$, $k_4 = 1.0$, $c_s = 1$, $c_g = 0$), $\sigma = k_2/k_4 = 0.04$

Figure 3: Our model is able to reproduce scalability dynamics described by the existing models: (a, b) Gustafson's law, and (c, d) Amdahl's law. Plots on the left show the number of units by their states with the increase of the system size N. Plots on the right show the speedup S_{thruput} as a function of N. In the ideal concurrency situation, (a, b), S_{thruput} unboundedly increases by increasing N; in the contention-limited regime, (c, d), S_{thruput} saturates to a constant value for large N. The value of the rates are indicated below the plots, unspecified rates are set to zero.

keeping $k_i = 0$ for $i \in \{2, 3, 5, 6, 7\}$. In this case, by computing the stable fixed point of Eq. (12) (see Appendix) we obtain

$$S_{\text{thruput}}(N) = \frac{\sqrt{k_4^2 + 8k_1 k_4 N} - k_4}{4k_1}, \tag{17}$$

which approximates the dynamics of Gustafson's law for $k_4 > k_1$. Figure 3b shows a representative configuration of Eq. (17) for $k_1 = 0.002$ and $k_4 = 1$. Similarly to Gustafson's law, Eq. (17) sublinearly grows with the system size N without saturating, even for large N.

3.2 Contention-limited – Amdahl's law

Amdahl's law (Eq. (1)) describes the scalability dynamics where the performance increase is limited by interaction cost. In fact, S_{thruput} increases with the system size N until a saturation limit, after which the performance stays constant with increasing system size N. Gunther's USL (Eq. (3)) can also describe such dynamics by setting the contention parameter $\sigma > 0$ and the coherency delay parameter $\kappa = 0$. Our model reproduces such dynamics for $k_1 > 0$, $k_2 > 0$ and $k_4 > 0$, while keeping $k_i = 0$ for $i \in \{3, 5, 6, 7\}$ (see details in the Appendix). As a difference from the ideal concurrency case (Sec. 3.1), in this scenario the interference has a relatively strong positive feedback (rate k_2) that limits the increase of performance with N.

In the Appendix, we show that for the special case $k_2 = 2k_1$ the stable fixed point (s^*, g^*, f^*) yields

$$S_{\text{thruput}}(N) = \frac{N}{1 + \frac{k_2}{k_4}N} \quad . \tag{18}$$

This equation has the same form as Amdahl's law of Eq. (1) suggesting that the serial part parameter $\sigma = \frac{k_2}{k_4}$. On the one hand, increasing rate k_4 in our model corresponds to decreasing the serial part of the task in Amdahl's law. In our model, k_4 dictates how frequently units complete interactions (*i.e.*, leave state *grupo* G and return to *solo* S), and by increasing k_4, the interaction cost decreases. On the other hand, the interaction feedback k_2 increases the rate of units moving to state G, and by removing it ($k_2 = k_1 = 0$) the model reduces to the ideal concurrency case of Sec. 3.1.

Figs. 3c and d show the results for $k_1 = 0.004$, $k_2 = 0.04$, and $k_4 = 1.0$ that resemble Amdahl's law dynamics of Fig. 1a. Note that in region $N < \frac{k_4}{k_2}$ the performance does not saturate because units complete interactions at a rate faster than interactions take place, leading to a permanently increasing performance. For $N > \frac{k_4}{k_2}$ the curve $S_{\text{thruput}}(N)$ starts flattening, and for $N \to \infty$ Eq. 18 converges to $S_{\text{thruput}}(N) \approx \frac{k_4}{k_2}$.

3.3 Diminishing returns

In the diminishing returns regime, the system increases in performance with increasing N until the critical value N_c. Increasing the system size beyond the critical value, $N > N_c$, leads to a decrease in performance due to an increase of the coordination costs. Gunther's USL describes such dynamics with the coherency delay parameter $\kappa > 0$ (regardless of the contention parameter's value σ). In our model, the diminishing returns regime is the result of feedbacks by units in states *grupo* G and *fermo* F that cause the transition of more and more units to these (here unproductive) states. By setting every rate $k_i > 0$ for $i \in \{1, ..., 7\}$, the system can go in a diminishing returns regime. While we were able to find the symbolic function of the stable fixed points, they were intractable because they are too long and cannot provide any analytical benefit. However,

15

in the Appendix, we show that fixing the rates $k_2 = k_3 = k_5 = k_6 = 2k_1$ and $k_4 = k_7$, and through an approximation, we find

$$S_{\text{thruput}}(N) = \frac{N}{\frac{k_2^2}{k_4^2}N^2 + \frac{k_2}{k_4}N + 1} \ . \tag{19}$$

Interestingly, our model as given in Eq. (19) and being derived from a microscopic model of interactions among units is similar to Gunther's USL of Eq. (3). The parameters are linked as $\sigma = \frac{k_2}{k_4}$ (in line with what has been discussed in Sec. 3.2) and $\kappa = \frac{k_2^2}{k_4^2} = \sigma^2$. The parameters κ and σ are not restricted in this way in the original USL. Gunther et al. [Gunther et al., 2015a] allow both positive and negative contention parameters σ, depending on the system's characteristics, to describe positive or negative contention (see also Sec. 3.4). By argument of symmetry one can ask if also the coherency delay parameter κ should accept negative values to represent a form of 'negative lack of coherence', or in other words, a form of super-coherence. However, according to Eq. (19) we have $\kappa = \frac{k_2^2}{k_4^2} = \sigma^2$ prohibiting negative values. Fig. 4 shows an example of the diminishing returns regime. Such system dynamics have been reported in parallel computing [Gunther, 1993] as well as in multi-robot scenarios [Hamann, 2018a].

3.4 Superlinear speedup

As reported by Gunther et al. [Gunther et al., 2015a], certain systems can benefit from interactions between units to achieve a superlinear speedup of performance. Such a scenario is particularly relevant in multi-robot systems in which robots may be able to cooperate with each other to improve their performance to a greater extent than they would do by executing the task independently (*e.g.*, [Berman et al., 2011, Ijspeert et al., 2001, O'Grady et al., 2007, Talamali et al., 2020]). For example, in a collective resource collection task (*e.g.*, based on pheromone trails [Talamali et al., 2020]), a single robot may take long time to find the unknown location of the resource cluster. Conversely, groups of robots can share information on individual searches and superlinearly speedup the collective task.

In our model, the beneficial or detrimental nature of the interactions is specified via the contribution coefficients. Values of c_g that are larger or smaller than c_s indicate that units are more productive in state *grupo* or *solo*, respectively. With $c_g < c_s$, each unit in state G is less effective than units in state S, therefore interactions should be minimized to improve the performance. On the contrary, $c_g > c_s$ indicates that interacting units, in state G, are more effective than units operating independently, therefore interactions should be maximized to improve performance. Note that how beneficial (or detrimental) states are, is independent from the details of the population dynamics (transition rates k_i). Fig. 4 shows such an example: the same underlying population

(a) states of the units

(b) speedup S_{thruput} based on *solo* S, $c_s = 1$, $c_g = 0$

(c) speedup S_{thruput} based on *solo* S and *grupo* G, $c_s = 1$, $c_g = 8$
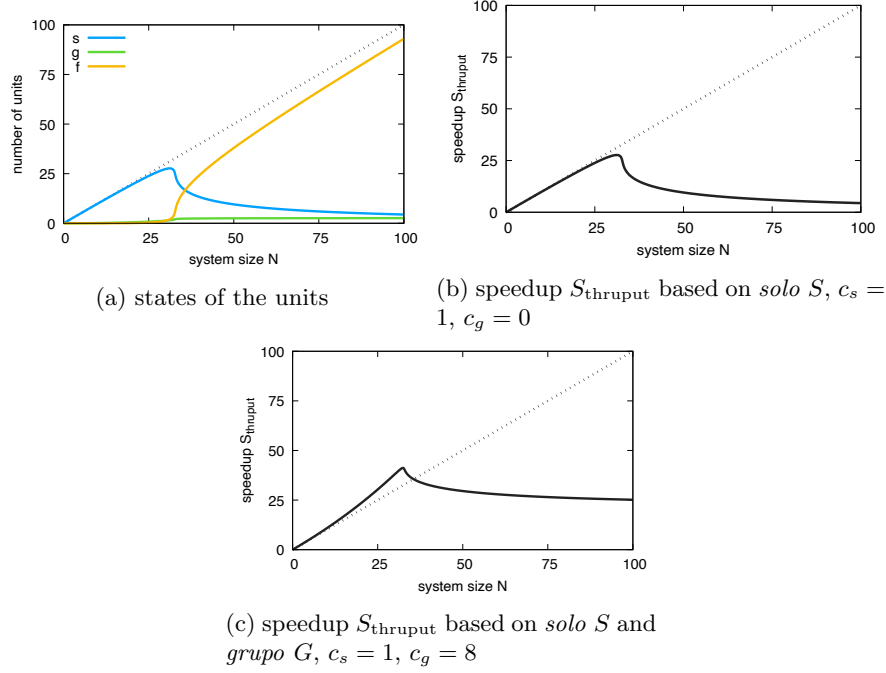
Figure 4: The same population dynamics (panel (a) with rates from Tab. 1) can give (b) diminishing returns or (c) superlinear speedup, depending on the coefficient parameters. In (b), $c_s = 1$, $c_g = 0$ indicate that the system benefits from *solo* units only. Instead, in (c), $c_s = 1$, $c_g = 8$ indicate that units in state *grupo* are eight times more efficient than *solo* units, leading to a superlinear speedup (when the curve is above the dashed diagonal).

dynamics (Fig. 4a with parameters of Tab. 1) can lead to two different speedup curves (Figs. 4b and 4c) as a consequence of different contribution coefficients. Superlinear speedups are observed when beneficial interactions among units cause the performance of a system of N units to be $S_{\text{thruput}} > N$. Gunther's USL can model superlinear speedups by setting the contention parameter to negative values, $\sigma < 0$, as it represents beneficial interactions. Our model can show superlinear speedups when the ratio of the contribution coefficients $\frac{c_g}{c_s}$ is larger than one, as indicated in Eq. (16). When the *grupo* coefficient c_g is larger than the *solo* coefficient c_s, then collaborating units in state *grupo* are more effective than *solo* units. Therefore, the system throughput of N units can be greater than N-times the throughput c_s of a single unit. In our model, superlinear speedup is a combination of the task's characteristic—that is, the benefits of collaboration—and of the system's functioning—that is, the number of units that collaborate with each other.

17

|	
k_1	0.005
k_2	0.1
k_3	0.06
k_4	10
k_5	0.15
k_6	0.3
k_7	0.8

Table 1: Transition rates for diminishing returns and superlinear speedup shown in Fig. 4.

4   Showcase: model fitting

In order to showcase the wide applicability of the proposed approach, we fit our scalability model to published data from three different fields: parallel computing, wireless sensor networks, and multi-robot systems. Obtaining a good fit is an indicator of how the model could potentially reproduce the dynamics observed in parallel and distributed systems. In the considered systems, the task is performed by units in state *solo* only, therefore we set the contribution coefficients of Eq. 15 to $c_s > 0$ and $c_g = 0$. The value of c_s is determined for each task as $X(1) = c_s$ (following the discussion in Sec. 2.3). While we set the contribution coefficients this way by hand based on our interpretation of the tasks, we automated the identification of the transition rates of Eqs. (5) to (11) through a fitting routine. We fit the performance function $X(N)$ of Eq. (15) to the performance data taken from the literature. As $X(N)$ depends on the stable fixed point of the system of Eq. (12), we numerically computed it through time integration with starting point $s(0) = N$, $g(0) = 0$, $f(0) = 0$. As fitting routine, we employed the differential evolution method [Storn and Price, 1997] implemented in SciPy [Virtanen et al., 2020].

We show that our model can fit data from the following four distinct systems: an SQL server benchmark on a multiprocessor machine, a media access protocol in a wireless sensor network, a simulation of self-propelled particles, and a simulation of a robot swarm performing the foraging task. In this section, we describe in more detail the four systems and briefly discuss the obtained fits. The fitted transition rates for the four studied systems are reported in Tab. 2, which also includes the contribution coefficient c_s used to scale throughput $X(N)$ to the data range. Fig. 5 shows the data superimposed to state curves for the fitted transition rates. While the fit has been done on the throughput $X(N)$, we plot the fixed point of the three states because it gives some additional information about the other states and, in the studied cases, the plot for the *solo* units is directly proportional to $X(N) = c_s \, s^*$ (with $c_s > 0$ and $c_g = 0$). For simplicity, we also normalize system size N (horizontal axis of Fig. 5) with linear scaling setting the first data point to $N = 1$.
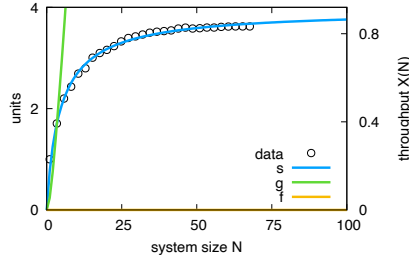
The data of the SQL server benchmark have been taken from [Gunther, 2007]. The performance data are the transactions per second, and the system size is
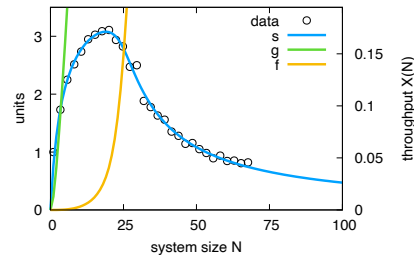
18
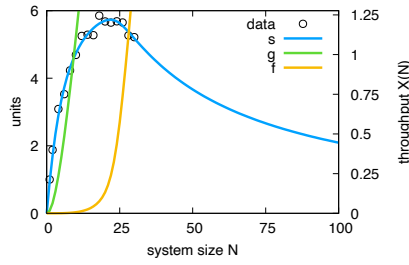
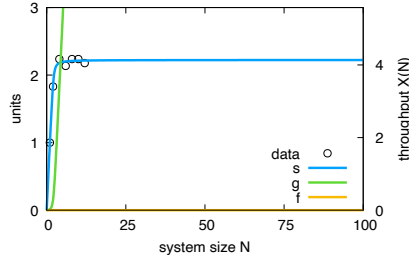(a) SQL Server, dataset from Gunther [Gunther, 2007]
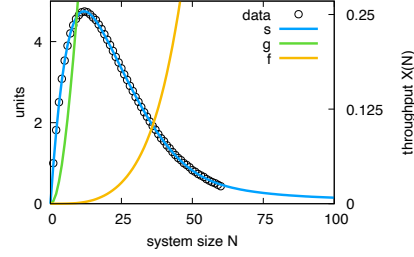
(b) wireless network with ALOHA protocol, dataset from Gokturk et al. [Gokturk et al., 2008]
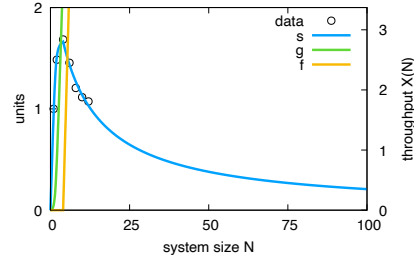

(c) foraging self-propelled particles (going through each other), dataset from Rosenfeld et al. [Rosenfeld et al., 2006]

(d) foraging robot swarm (embodied system), dataset from Rosenfeld et al. [Rosenfeld et al., 2006]

(e) NAS parallel benchmark, Block Tridiagonal (BT), dataset from Ribeiro et al. [Ribeiro et al., 2012]

(f) NAS parallel benchmark, Scalar Pentadiagonal (SP), dataset from Ribeiro et al. [Ribeiro et al., 2012]

Figure 5: Fitting Eqs. 12 and 15 to datasets from parallel computing [Gunther, 2007], wireless networks [Gokturk et al., 2008], and swarm robotics [Rosenfeld et al., 2006]. For simplicity all horizontal axes are normalized to the range $N \in [1, 100]$. The fitted parameters are given in Tab. 2.

the number of virtual users ($N \in \{1, 2, \ldots, 30\}$). The published data includes results for different hardware configurations, we focus on the '4-way processor configuration' data. The fitting results of Fig. 5a indicate a good fit. Interpreting the fitted parameters of Tab. 2 is nontrivial. However, we notice that the

19

ratio between rate k_4 and rate k_2 predicts an increase of $X(N)$ for $N \leq 7$ (as $\frac{k_4}{k_2} \approx 7$) approximately, as shown in Fig. 5a. Additionally, rates $k_3, k_5, k_6 > 0$ indicate that units may eventually arrive to state *fermo* anticipating diminishing returns for large N.

Next, we fit data of a wireless sensor network that applies a common protocol for media access called ALOHA, the data have been taken from [Gokturk et al., 2008]. The performance data is the throughput, measured as number of packets per slot (numerical results), and the system size is the number of backlogged nodes. The results shown in Fig. 5b indicate a good fit. By looking at the fitted transition rates in Tab. 2, we note that rate k_3 is significantly larger than all other rates (except for k_7). This rate triggers state transitions from state *solo* to state *grupo* depending on the number of units in *fermo*. This rate hence causes the steep decline in performance for $N > 13$ when media access quickly gets more difficult due to congestion.

The self-propelled particle system is composed of a group of units that can move in bidimensional space without any collision among them. The data have been taken from [Rosenfeld et al., 2006] (algorithm *goThru*). The self-propelled particles perform the swarm robotics benchmark of *foraging*, that is, they are tasked to collect items scattered in the environment and transport them to a central location. The particles locally communicate with each other in order to coordinate the foraging operation. The performance data are the number of collected items and the system size is the number of particles. As the particles can go through each other there is no physical interference among them. In this case, the limiting resource is the number of available items that leads the system performance to saturate to a fixed value for large N, in a way similar to Amdahl's law. Due to the lack of interference, we set $k_5 = k_6 = 0$ to turn off state *fermo*, see Tab. 2. The results shown in Fig. 5c indicate a good fit. As expected, the curve saturates for large N.

We study another system, this one is a robot swarm. The data have been taken from [Rosenfeld et al., 2006] (algorithm *timeRand*). The robots perform the same foraging task of the previous system. However, in this system, the robots cannot go through each other's bodies and therefore they may physically interfere with the movements of one another. Due to physical interference, the expected scalability curve is diminishing performance for large system size N, as for large robot densities, room required to avoid collisions is limited. The results shown in Fig. 5d indicate a good fit. Parameters k_5 and k_6 (transition $G \rightarrow F$) are small relative to k_1, k_2, k_3 to model the late but steep decline on the interval $24 < N < 60$. Note that the shapes of $X(N)$ in Fig. 5b and Fig. 5d seem similar but in the swarm robotics system there is first a saturation for $N \approx 20$ and then a steep decline indicating a different underlying process.

Finally, we study two more datasets from parallel computing to include more representative parallel applications. Both applications are from the NAS Parallel Benchmark [Jin et al., 1999]. The benchmark is based on a number of tasks for computational fluid dynamics. Here, we focus on two of them: BT and SP. Task BT is based on an algorithm to solve 3-dimensional compressible Navier-Stokes equations that form block-tridiagonal (BT) systems. Task SP is

param.	SQL server	wireless netw.	self-prop. part.	robot swarm	NAS BT	NAS SP
k_1	0.1600614759	0.02889861707	1.390301954	1.475881283	0.03415882417	0.0987250043
k_2	0.5640057846	0.1316419438	2.152415749	2.262085575	4.001963225	4.63175441
k_3	0.3054490761	6.119334033	0	4.859955018	0	0.804438853
k_4	4.058864868	0.9700209090	8.499633576	9.341897861	8.899802172	7.93215055
k_5	0.003989433297	0.003321168620	0	0.002558004976	0	$3.73031451 \times 10^{-9}$
k_6	0.5243111486	0.1970954618	0	0.3318341624	0	4.20617254
k_7	9.567349145	9.898300316	0	7.214769884	0	9.83304445
c_s	0.212894142	0.05369458128	0.276059326	0.219971588	1.988764045	1.727748691
MSE	8.21545×10^{-4}	1.21005×10^{-6}	2.42738×10^{-4}	2.77502×10^{-4}	6.18738×10^{-3}	4.37801×10^{-3}

Table 2: Fitted parameters for six different systems: multiprocessor SQL server, wireless network, self-propelled particles, robot swarm, NAS Parallel Benchmark Block Tridiagonal (BT) and scalar Pentadiagonal (SP); results are shown in Fig. 5. The row 'MSE' indicates the mean squared error from the data points.

based on a similar problem but solves scalar pentadiagonal (SP) bands of linear equations. We rely on benchmark data from Ribeiro et al. [Ribeiro et al., 2012]. They investigate the impact of different architectures for shared memory but we focus only on their data for uniform memory access (UMA) using a machine with four six-core Intel Xeon X7460 and Linux 2.6.32. We fit their data "Intel UMA" for BT and SP of speedup over number of cores (see Figs. 5e and 5f). For task BT, the system performance saturates as seen previously for the self-propelled particle system in Fig. 5c. According to Ribeiro et al. [Ribeiro et al., 2012] this may be caused by memory issues and thread migrations. Similar to the case of the self-propelled particle system, we set $k_5 = k_6 = 0$ to turn off state *fermo*, see Tab. 2. For task SP, We observe diminishing performance for too large system size N. According to Ribeiro et al. [Ribeiro et al., 2012] this may be caused by memory issues and non-continuous communication. For both tasks the results in Figs. 5e and 5f indicate good and reasonable fits despite the few available data points (seven each).
As already discussed, one of the advantages of our model is the link between the state of units with the performance curve. By investigating the casual effect of each rate on the system performance, we can achieve a better understanding of the system behavior. However, in this paper we leave out any articulated discussion on the rates and in depth interpretation of the causes of the observed scalability curves. We will refer to this in future work. Also, we would like to draw attention to the further advantage of having a unified model applicable to systems of different fields that allows the identification of similarities and analogies among, apparently different, fields.

5 Conclusion

We have presented a new general model to study scalability of parallel systems composed of multiple units (*e.g.*, supercomputer composed of CPUs, and artificial swarms composed of robots). Our model covers all relevant scenarios of ideal concurrency, contention-limited systems, and diminishing returns. In addition, our model is derived from a microscopic description of state transitions of the units comprising the system. The units can be in three states that change

over time due to interactions with other units. The model can be represented as a probabilistic state machine that describes the mean behavior of a unit (*microscopic* model). From the individual state machine, we show how to derive the *macroscopic* population model that describes the scalability behavior of the whole system. The derivation of the model from the mechanistic description of interactions between the constituent units is one of the main differences with previous scalability laws. Amdahl's law and Gustafson's law are phenomenological models that are not derived from first principles. Gunther's USL is well motivated by queuing theory but is still based on phenomenological assumptions, such as nonlinear waiting times in the state-dependent server model. Our model has more explanatory power by providing a direct link between system behavior and microscopic behaviors of its units. However, increased explanatory power comes with the cost of higher model complexity. The model has nine parameters: the seven transition rates that describe the frequency of state change by the units, and the two contribution coefficients that describe the work contributed by a solitary and an interacting unit towards task completion. While the number of parameters is larger than in previous models, the separation between transition rates k_i (mechanistic function) and contribution coefficients c_s, c_g (task-specific performance) allows a better understanding of the observed scalability behavior. For example, we interpret the cause of superlinear speedups as discussed in Sec. 3.4.

The transition rates k_i of a system can be determined in two alternative ways: by fitting the rates to system data (as shown in Sec. 4) or by observing and measuring individual transitions. While fitting parameters operates on data at the macroscopic level (system performance), measuring individual transitions represents a microscopic approach. Individual transition rates can be obtained in systems that control the units using finite state machines, or behaviors, that may be mapped to our model's state machine. In a robot swarm, for example, robots can be assigned to state *fermo* when their internal control state is *robot-avoidance* due to physical proximity to other robots. The problem of finding the correct model parameters is a special form of nonlinear system identification for gray-box models [Nelles, 2013]. Transition rates can potentially be estimated or even computed by either measuring the time spent by each unit in productive, collaborative, and unproductive states or by observing and counting individual state transitions. For instance, in a computing system, idle and busy times can be measured to estimate transition rates. A better approach would be to count individual transitions while keeping track of populations in each state at the time of the observed transition. Hence, complex machine behaviors can be simplified to observable state transitions between our simple three states (*solo*, *grupo*, *fermo*), which allows to determine the model parameters. Based on our model and estimated rates k_i, one can then predict the system behavior and study its potential for scalability.

We have focused on the asymptotic behavior (*i.e.*, at equilibrium) of the system, however the analysis can be extended to the system's transient dynamics before reaching equilibrium. Such an analysis could potentially provide additional information to improve the system design. Similarly to previous models of

scalability, our model is also limited to static systems that do not vary the number of units (*e.g.*, in robotics see [Buyya et al., 2009, Wahby et al., 2019, Mayya et al., 2019, Rausch et al., 2019]) or the task (*e.g.*, [Matarić et al., 2003]) at runtime. Our model, however, has potential to be extended for such cases by modifying the state transitions to include 'birth' and 'death' of units (system size variation), and by introducing time-varying parameters (dynamic tasks). Such features may be relevant in open systems where units are added and removed online, for example, in on-demand cloud computing which is based on dynamic use of resources [Buyya et al., 2009].

Our approach of starting from the description of changes of an individual unit's state to derive a macroscopic model is common practice in swarm robotics [Martinoli, 1999, Reina et al., 2015, Hamann, 2018b] and collective behavior studies [Marshall et al., 2019]. Such an approach follows the line of thought of *machine behavior* [Rahwan et al., 2019] that advocates the necessity to understand the cause of its behavior in order to fully control the machine. For example, the current efforts towards blackbox approaches in artificial intelligence require a new interdisciplinary approach in order to progress. In this study, we show that through a collective behavior approach, we could contribute to the understanding of parallel computing. Additionally, we contribute towards a unified description of systems in diverse areas such as parallel computing, sensor networks, and swarm robotics. In future work, we plan to study whether our general model can also describe systems from other fields. In addition, other unified models to describe engineering systems could be derived through ethology and behavioral ecology methods, as it is commonly done in swarm robotics [Hamann, 2018b]. Deeper insights may be obtained by studying scalability of systems with a set of interdisciplinary methods and with models of wide applicability.

Acknowledgments

---

[4] http://www.gnuplot.info/
[5] https://www.gnu.org/software/emacs/
[6] https://automeris.io/WebPlotDigitizer/
[7] https://www.overleaf.com/

Appendix

Stability analysis

Our model, described as an ODE system in Eq.(12) of the main text, is derived from the seven transitions of Eqs. (5)-(11) using van Kampen's expansion [van Kampen, 1981]. Therefore, the terms s, g, and f indicate unit concentrations $s = |S|/V$, $g = |G|/V$, and $f = |F|/V$, where $|S|$, $|G|$, and $|F|$ are the number of units in each of the three states *solo*, *grupo*, and *fermo*, respectively, and the term V is the system volume. As we are interested in studying the population dynamics for increasing concentrations of units for a fixed volume, for simplicity we fix $V = 1$. Therefore, in our analysis, the concentrations s, g, and f are equivalent to the population sizes $|S|$, $|G|$, and $|F|$.

In our model, the system size N is conserved, that is, the system units only change state but do not change in number (no birth or death); mathematically indicated by $N = f + m + c$. Therefore, we can rewrite the ODE system of main text Eq. (12) by substituting the subpopulation of units in state G with $g = N - s - f$. This substitution allows us to remove the second ODE. The resulting ODE system is

$$\begin{cases} \dfrac{ds}{dt} = -2k_1 s^2 - k_2 s(N - s - f) - k_3 sf + k_4(N - s - f) \\ \dfrac{df}{dt} = 2k_5(N - s - f)^2 + k_6 f(N - s - f) - k_7 f \end{cases} . \tag{20}$$

Writing the model in the form of Eq. (20) has two advantages compared to main text Eq. 12. Having a system of two equations, instead of three, simplifies its analysis. The ODE system now explicitly includes the system size, as parameter N.

By varying transition rates k_i (for $i \in \{1, \ldots, 7\}$), we show how our general model can flexibly approximate the dynamics of previous scalability laws, in particular of Gustafson's, Amdahl's, and Gunther's laws. Note that we assume that initially (at time $t = 0$) the system has only *solo* units:

$$s(0) = N, \qquad g(0) = 0, \qquad f(0) = 0. \tag{21}$$

Gustafson's law: the ideal concurrency regime

We set $k_2 = k_3 = k_5 = k_6 = k_7 = 0$, and we only keep $\{k_1, k_4\} > 0$. In this way, Eq. (20) reduces to the single ODE

$$\frac{ds}{dt} = -2k_1 s^2 + k_4(N - s - f), \tag{22}$$

because $\frac{df}{dt} = 0$. This equation has a single stable fixed point at

$$s^* = \frac{\sqrt{k_4(k_4 + 8k_1 N)} - k_4}{4k_1}, \tag{23}$$

and we have $g^* = N - s^*$ and $f^* = 0$.

Amdahl's law: the contention-limited regime

We set $k_3 = k_5 = k_6 = k_7 = 0$, and we only keep $\{k_1, k_2, k_4\} > 0$. The only difference from Gustafson's law is $k_2 > 0$ that corresponds to the transition $S + G \to 2G$ from main text Eq. 6. As before, from the ODE system of Eq. (20) we obtain a single equation (because $\frac{df}{dt} = 0$):

$$\frac{ds}{dt} = -2k_1 s^2 - k_2 s(N - s - f) + k_4(N - s - f) , \qquad (24)$$

which has a single stable fixed point at

$$s^* = \frac{k_4 + k_2 N - \sqrt{k_4^2 + 8k_1 k_4 N - 2k_2 k_4 N + k_2^2 N^2}}{2(-2k_1 + k_2)} . \qquad (25)$$

This fixed point always exists, except for $k_2 = 2k_1$ due to a singularity and the fixed point of the system becomes

$$s^* = \frac{k_4 N}{k_4 + k_2 N} . \qquad (26)$$

As before, in both Eq. (25) and Eq. (26), we have $g^* = N - s^*$ and $f^* = 0$. In this case, when the recruitment k_2 is relatively high, the *solo* fraction grows with system size N only for small values, smaller than N_c. Beyond N_c, it saturates to a value that decreases with k_2/k_4 (see Fig. 6 for examples)

The diminishing returns regime

We observe diminishing returns when the performance decreases with the system size N for $N > N_c$. If we assume performance coefficients $c_s = 1$ and $c_g = 0$, this type of behavior occurs when the number of units in the state *solo* increases for small values of N and collapses for high N. Interpreting the system's behavior through its dynamics (*cf.* Figs. 7 and 8), we expect to observe diminishing returns when *solo* units relatively slowly move to state *grupo* (small rates k_1 and k_2), while they relatively quickly move to state *fermo* (high rates k_5 and k_6). Mathematically, we can indicate that when $k_5 + k_6 > k_1 + k_2$ we observe the diminishing results regime. Therefore, we study the system with the following parameters:

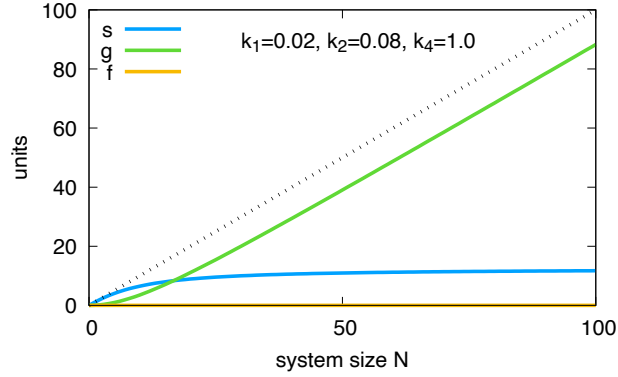$$k_2 = k_3 = k_5 = k_6 = 2k_1, \qquad k_4 = k_7 , \qquad (27)$$

which means that the crowding rate is double the interaction rate between *solo* units (k_1). Additionally, we simplify the analysis by imposing the same decay from states *grupo* and *fermo*. Using the parameters of Eq. (27), the stable fixed
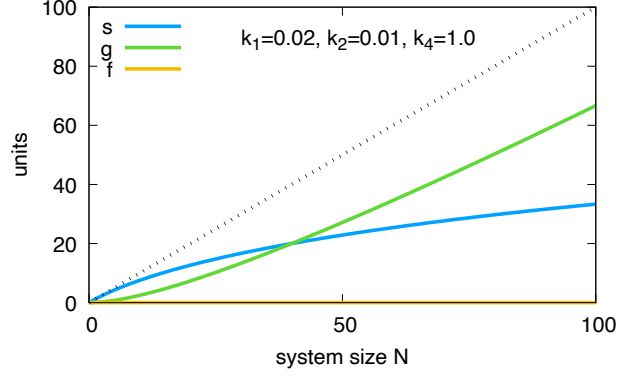
(a) crowding rate $k_2 = 0.01 = \frac{k_1}{2}$, $k_4 = 1.0$
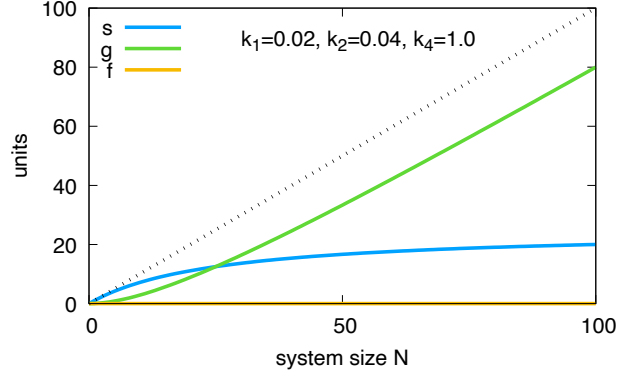
(b) crowding rate $k_2 = 0.04 = 2k_1$, $k_4 = 1.0$

(c) crowding rate $k_2 = 0.08 = 4k_1$, $k_4 = 1.0$

Figure 6: Amdahl's law: Increasing the positive feedback of crowding (k_2), in a system with simple interference (k_1) and decay (k_4), flattens the fraction of *solo* units for increasing system size N.

points of the ODE system of Eq. (20) is

$$s^* = \frac{2k_4^2 N}{4k_1^2 N^2 + \sqrt{16k_1^4 N^4 + 48k_4 k_1^3 N^3 - 4k_4^2 k_1^2 N^2 + 4k_4^3 k_1 N + k_4^4} + 2k_4 k_1 N + k_4^2}$$

$$f^* = -\frac{24k_1^3 N^3 - (2k_1 N + k_4)\sqrt{16k_1^4 N^4 + 48k_4 k_1^3 N^3 - 4k_4^2 k_1^2 N^2 + 4k_4^3 k_1 N + k_4^4} + 4k_4^2 k_1 N + k_4^3}{8k_1^2 k_4 N - 16k_1^3 N^2}$$

$$g* = N - s^* - f^* \ .$$

(28)

Fig. 7 shows three examples of the dynamics of Eq. (28). The reduction in *solo* units is more pronounced for higher crowding rates, as illustrated in Fig. 8.
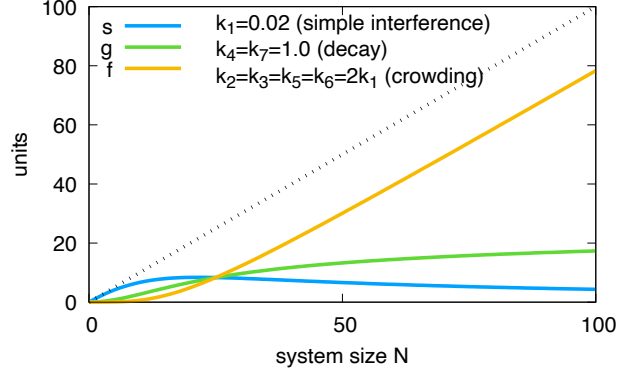
Approximation   For the above diminishing returns scenario (Eq. 28), we can approximate

$$16k_1^4 N^4 + 48k_4 k_1^3 N^3 - 4k_4^2 k_1^2 N^2 + 4k_4^3 k_1 N + k_4^4$$
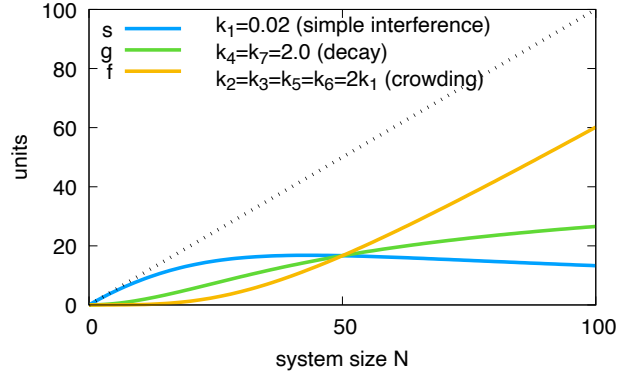$$\approx \left(4k_1^2 N^2 + 2k_4 k_1 N + k_4^2\right)^2 \ .$$

(29)

In this way, the first equation of Eq. (28) reduces to

$$s^* = \frac{N}{\frac{k_2^2}{k_4^2} N^2 + \frac{k_2}{k_4} N + 1} \ ,$$
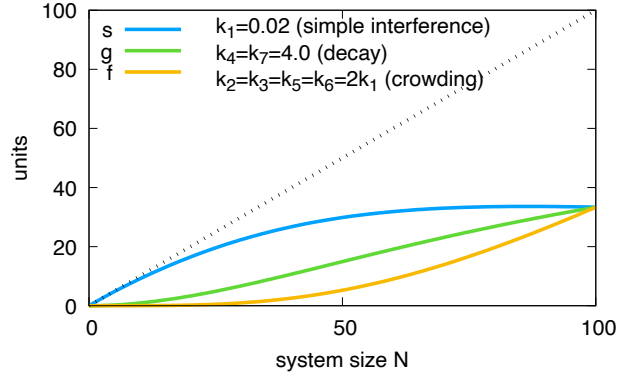
(30)

which closely corresponds to the Gunther's USL (main text Eq. 3) by considering $\kappa = \sigma^2$ and $\sigma = \frac{k_2}{k_4}$.

(a) decay rate $k_4 = k_7 = 1.0$

(b) decay rate $k_4 = k_7 = 2.0$

(c) decay rate $k_4 = k_7 = 4.0$

Figure 7: Examples for diminishing returns. By increasing the frequency of the decay rates k_4 and k_7, an increasing fraction of units stabilizes in state *solo*.
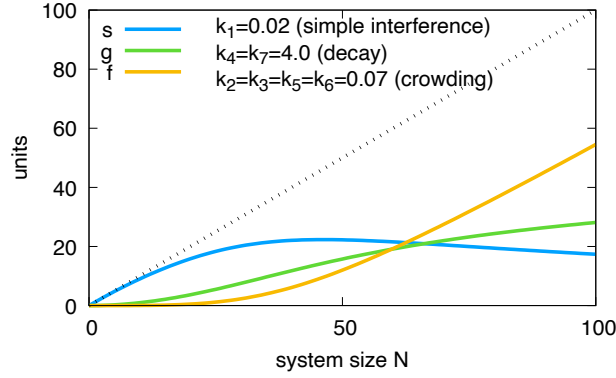
Figure 8: Example of diminishing return regime. By increasing system size N beyond ≈ 40 units, the number of units in state *solo* decreases. Assuming contribution coefficients $c_s = 1$ and $c_g = 0$, the system's performance would also decrease. Compared to Fig. 7c, a higher value of the 'crowding' rates leads to an earlier and more pronounced decrease of s.

References

A. O. Allen. *Probability, Statistics, and Queueing Theory with Computer Science Applications*. Academic Press Professional, Inc., USA, 1990. ISBN 0120510510.

G. M. Amdahl. Validity of the single processor approach to achieving large scale computing capabilities. In *AFIPS Conference Proceedings*, pages 483–485. ACM, 1967.

J. Archibald and J.-L. Baer. Cache coherence protocols: Evaluation using a multiprocessor simulation model. *ACM Transactions on Computer Systems (TOCS)*, 4(4):273–298, 1986.

ASF - Apache Software Foundation. Apache hadoop. http://hadoop.apache.org.

G. Ballard, J. Demmel, O. Holtz, and O. Schwartz. Minimizing communication in numerical linear algebra. *SIAM Journal on Matrix Analysis and Applications*, 32(3):866–901, 2011.

S. Berman, Q. Lindsey, M. S. Sakar, V. Kumar, and S. C. Pratt. Experimental study and modeling of group retrieval in ants as an approach to collective transport in swarm robotic systems. *Proceedings of the IEEE*, 99(9):1470–1481, Sept 2011. ISSN 0018-9219. doi: 10.1109/JPROC.2011.2111450.

C. Bettstetter. On the connectivity of Ad Hoc networks. *The Computer Journal*, 47(4): 432–447, 2004.

J. D. Bjerknes and A. F. T. Winfield. On fault tolerance and scalability of swarm robotic systems. In M. Ani Hsieh and G. Chirikjian, editors, *Distributed Autonomous Robotic Systems: The 10th International Symposium*, volume 104 of *Springer Tracts in Advanced Robotics*, pages 431–444. Springer Berlin Heidelberg, Berlin, Heidelberg, 2013. doi: 10.1007/978-3-642-32723-0_31.

J. D. Bjerknes, A. Winfield, and C. Melhuish. An analysis of emergent taxis in a wireless connected swarm of mobile robots. In Y. Shi and M. Dorigo, editors, *IEEE Swarm Intelligence Symposium*, pages 45–52, Los Alamitos, CA, 2007. IEEE Press.

P. Bogdan and R. Marculescu. Statistical physics approaches for network-on-chip traffic characterization. In *Proceedings of the 7th IEEE/ACM International Conference on Hardware/Software Codesign and System Synthesis*, CODES+ISSS '09, page 461–470, New York, NY, USA, 2009. Association for Computing Machinery. ISBN 9781605586281. doi: 10.1145/1629435.1629498. URL https://doi.org/10.1145/1629435.1629498.

P. Bogdan and R. Marculescu. Non-stationary traffic analysis and its implications on multicore platform design. *IEEE Transactions on Computer-Aided Design of Integrated Circuits and Systems*, 30(4):508–519, apr 2011. ISSN 0278-0070. doi: 10.1109/TCAD.2011.2111270. URL http://ieeexplore.ieee.org/document/5737846/.

R. Buyya, C. S. Yeo, S. Venugopal, J. Broberg, and I. Brandic. Cloud computing and emerging it platforms: Vision, hype, and reality for delivering computing as the 5th utility. *Future Generation computer systems*, 25(6):599–616, 2009.

T. Dumitras and R. Marculescu. On-chip stochastic communication [soc applications]. In *2003 Design, Automation and Test in Europe Conference and Exhibition*, pages 790–795. IEEE, 2003.

J. H. Espenson. *Chemical kinetics and reaction mechanisms*, volume 102. McGraw-Hill, 1995.

K. Farkas, Z. Vranesic, and M. Stumm. Scalable cache consistency for hierarchically structured multiprocessors. *The Journal of Supercomputing*, 8(4):345–369, 1995.

M. Feng, L.-J. Deng, F. Chen, M. Perc, and J. Kurths. The accumulative law and its probability model: an extension of the pareto distribution and the log-normal distribution. *Proceedings of the Royal Society A: Mathematical, Physical and Engineering Sciences*, 476(2237): 20200019, 2020. doi: 10.1098/rspa.2020.0019. URL https://royalsocietypublishing.org/doi/abs/10.1098/rspa.2020.0019.

S. Garnier, J. Gautrais, and G. Theraulaz. The biological principles of swarm intelligence. *Swarm Intelligence*, 1:3–31, 2007. URL http://dx.doi.org/10.1007/s11721-007-0004-y.

D. T. Gillespie, A. Hellander, and L. R. Petzold. Perspective: Stochastic algorithms for chemical kinetics. *The Journal of Chemical Physics*, 138(17):170901, 2013. doi: 10.1063/1.4801941.

J. Gittins, K. Glazebrook, and R. Weber. *Multi-armed bandit allocation indices*. John Wiley & Sons, 1989.

M. S. Gokturk, O. Ercetin, and O. Gurbuz. Throughput analysis of ALOHA with cooperative diversity. *IEEE Communications Letters*, 12(6):468–470, 2008.

A. Grama, V. Kumar, A. Gupta, and G. Karypis. *Introduction to parallel computing*. Pearson Education, 2003.

N. J. Gunther. A simple capacity model of massively parallel transaction systems. In *CMG National Conf.*, pages 1035–1044, 1993.

N. J. Gunther. *Guerrilla Capacity Planning*. Springer, 2007.

N. J. Gunther. A general theory of computational scalability based on rational functions. *arXiv preprint arXiv:0808.1431*, 2008.

N. J. Gunther, P. Puglia, and K. Tomasette. Hadoop super-linear scalability: The perpetual motion of parallel performance. *ACM Queue*, 13(5), 2015a.

N. J. Gunther, P. Puglia, and K. Tomasette. Hadoop super-linear scalability. *Commun. ACM*, 58(4):46–55, 2015b.

J. L. Gustafson. Reevaluating Amdahl's law. *Commun. ACM*, 31(5):532–533, May 1988. ISSN 0001-0782. doi: 10.1145/42411.42415. URL http://doi.acm.org/10.1145/42411.42415.

J. L. Gustafson. Fixed time, tiered memory, and superlinear speedup. In *Proceedings of the Fifth Distributed Memory Computing Conference (DMCC5)*, pages 1255–1260, 1990.

H. Hamann. Towards swarm calculus: Urn models of collective decisions and universal properties of swarm performance. *Swarm Intelligence*, 7(2-3):145–172, 2013. URL http://dx.doi.org/10.1007/s11721-013-0080-0.

H. Hamann. Superlinear scalability in parallel computing and multi-robot systems: Shared resources, collaboration, and network topology. In M. Berekovic, R. Buchty, H. Hamann, D. Koch, and T. Pionteck, editors, *Architecture of Computing Systems – ARCS 2018*, pages 31–42, Cham, 2018a. Springer International Publishing. ISBN 978-3-319-77610-1.

H. Hamann. *Swarm Robotics: A Formal Approach*. Springer, Cham, 2018b. doi: 10.1007/978-3-319-74528-2.

D. P. Helmbold and C. E. McDowell. Modelling speedup (n) greater than n. *IEEE Transactions on Parallel and Distributed Systems*, 1(2):250–256, 1990.

A. J. Ijspeert, A. Martinoli, A. Billard, and L. M. Gambardella. Collaboration through the exploitation of local interactions in autonomous collective robotics: The stick pulling experiment. *Autonomous Robots*, 11:149–171, 2001. ISSN 0929-5593. doi: 10.1023/A: 1011227210047. URL http://dx.doi.org/10.1023/A%3A1011227210047.

H. Jin, M. Frumkin, and J. Yan. The OpenMP implementation of NAS parallel benchmarks and its performance. Technical Report NAS-99-011, NASA Ames Research Center, 1999.

Y. Khaluf, C. Pinciroli, G. Valentini, and H. Hamann. The impact of agent density on scalability in collective systems: noise-induced versus majority-based bistability. *Swarm Intelligence*, 11(2):155–179, Jun 2017. ISSN 1935-3820. doi: 10.1007/s11721-017-0137-6. URL https://doi.org/10.1007/s11721-017-0137-6.

D. B. Kirk and W. H. Wen-Mei. *Programming massively parallel processors: a hands-on approach*. Morgan kaufmann, 2016.

D. Lazer and A. Friedman. The network structure of exploration and exploitation. *Administrative Science Quarterly*, 52:667–694, 2007.

K. Lerman and A. Galstyan. A general methodology for mathematical analysis of multi-agent systems. *ISI-TR-529, USC Information Sciences Institute, Marina del Rey, CA*, 2001.

R. Mahnke and J. Kaupužs. Stochastic theory of freeway traffic. *Physical Review E*, 59(1): 117, 1999.

J. A. R. Marshall, A. Reina, and T. Bose. Multiscale modelling tool: Mathematical modelling of collective behaviour without the maths. *PLoS ONE*, 14(9):e0222906, 2019. doi: 10.1371/journal.pone.0222906.

A. Martinoli. *Swarm Intelligence in Autonomous Collective Robotics: From Tools to the Analysis and Synthesis of Distributed Control Strategies*. PhD thesis, Ecole Polytechnique Fédérale de Lausanne, 1999.

A. Martinoli, K. Easton, and W. Agassounon. Modeling swarm robotic systems: A case study in collaborative distributed manipulation. *Int. Journal of Robotics Research*, 23(4): 415–436, 2004.

M. J. Matarić, G. S. Sukhatme, and E. H. Østergaard. Multi-robot task allocation in uncertain environments. *Autonomous Robots*, 14(2-3):255–263, 2003.

S. Mayya, P. Pierpaoli, and M. Egerstedt. Voluntary retreat for decentralized interference reduction in robot swarms. In *Int. Conf. on Robotics and Automation (ICRA)*, pages 9667–9673. IEEE, 2019.

O. Nelles. *Nonlinear system identification: from classical approaches to neural networks and fuzzy models*. Springer Science & Business Media, 2013.

R. O'Grady, R. Gross, A. L. Christensen, F. Mondada, M. Bonani, and M. Dorigo. Performance benefits of self-assembly in a swarm-bot. In *IEEE/RSJ International Conference on Intelligent Robots and Systems (IROS)*, pages 2381–2387, Oct 2007. doi: 10.1109/IROS.2007.4399424.

I. Rahwan, M. Cebrian, N. Obradovich, J. Bongard, J.-F. Bonnefon, C. Breazeal, J. W. Crandall, N. A. Christakis, I. D. Couzin, M. O. Jackson, N. R. Jennings, E. Kamar, I. M. Kloumann, H. Larochelle, D. Lazer, R. McElreath, A. Mislove, D. C. Parkes, A. S. Pentland, M. E. Roberts, A. Shariff, J. B. Tenenbaum, and M. Wellman. Machine behaviour. *Nature*, 568(7753):477–486, 2019. doi: 10.1038/s41586-019-1138-y.

I. Rausch, A. Reina, P. Simoens, and Y. Khaluf. Coherent collective behaviour emerging from decentralised balancing of social feedback and noise. *Swarm Intelligence*, 13(3–4):321–345, 2019. doi: 10.1007/s11721-019-00173-y.

A. Reina, G. Valentini, C. Fernández-Oto, M. Dorigo, and V. Trianni. A design pattern for decentralised decision making. *PLoS ONE*, 10(10):e0140950, 2015. doi: 10.1371/journal.pone.0140950.

M. Resnick. *Turtles, Termites, and Traffic Jams*. MIT Press, 1994.

C. P. Ribeiro, M. Castro, V. Marangonzova-Martin, J.-F. Méhaut, H. C. de Freitas, and C. A. P. da Silva Martins. Evaluating CPU and memory affinity for numerical scientific multithreaded benchmarks on multi-cores. *IADIS International Journal on Computer Science and Information Systems (IJCSIS)*, 7:79–93, 2012.

L. G. Roberts. ALOHA packet system with and without slots and capture. *SIGCOMM Comput. Commun. Rev.*, 5(2):28–42, Apr. 1975. ISSN 0146-4833. doi: 10.1145/1024916.1024920. URL https://doi.org/10.1145/1024916.1024920.

A. Rosenfeld, G. A. Kaminka, and S. Kraus. A study of scalability properties in robotic teams. In P. Scerri, R. Vincent, and R. Mailler, editors, *Coordination of Large-Scale Multiagent Systems*, pages 27–51. Springer US, Boston, MA, 2006. ISBN 978-0-387-27972-5. doi: 10.1007/0-387-27972-5_2. URL https://doi.org/10.1007/0-387-27972-5_2.

H. Sayama, I. Pestov, J. Schmidt, B. J. Bush, C. Wong, J. Yamanoi, and T. Gross. Modeling complex systems with adaptive networks. *Computers & Mathematics with Applications*, 65 (10):1645–1664, 2013. ISSN 0898-1221. doi: https://doi.org/10.1016/j.camwa.2012.12.005. URL https://www.sciencedirect.com/science/article/pii/S0898122112007018. Grasping Complexity.

Y. Shang and R. Bouffanais. Influence of the number of topologically interacting neighbors on swarm dynamics. *Scientific Reports*, 4(4184), 2014.

R. Storn and K. Price. Differential evolution–a simple and efficient heuristic for global optimization over continuous spaces. *Journal of Global Optimization*, 11(4):341–359, 1997.

M. S. Talamali, T. Bose, M. Haire, X. Xu, J. A. R. Marshall, and A. Reina. Sophisticated collective foraging with minimalist agents: A swarm robotics test. *Swarm Intelligence*, 14 (1):25–56, 2020. doi: 10.1007/s11721-019-00176-9.

N. G. van Kampen. *Stochastic Processes in Physics and Chemistry*. North-Holland, Amsterdam, 1981.

P. Virtanen, R. Gommers, T. E. Oliphant, M. Haberland, T. Reddy, D. Cournapeau, E. Burovski, P. Peterson, W. Weckesser, J. Bright, S. J. van der Walt, M. Brett, J. Wilson, K. Jarrod Millman, N. Mayorov, A. R. J. Nelson, E. Jones, R. Kern, E. Larson, C. Carey, İ. Polat, Y. Feng, E. W. Moore, J. Vand erPlas, D. Laxalde, J. Perktold, R. Cimrman, I. Henriksen, E. A. Quintero, C. R. Harris, A. M. Archibald, A. H. Ribeiro, F. Pedregosa, P. van Mulbregt, and S. . . Contributors. SciPy 1.0: Fundamental Algorithms for Scientific Computing in Python. *Nature Methods*, 17:261–272, 2020. doi: https://doi.org/10.1038/s41592-019-0686-2.

M. Wahby, J. Petzold, C. Eschke, T. Schmickl, and H. Hamann. Collective change detection: Adaptivity to dynamic swarm densities and light conditions in robot swarms. In *Artificial life: A hybrid of the European conference on artificial life (ECAL) and the international conference on the synthesis and simulation of living systems (ALIFE)*, pages 642–649. MIT Press, 2019.

X. Zhang, G. Neglia, J. Kurose, and D. Towsley. Performance modeling of epidemic routing. *Computer Networks*, 51(10):2867–2891, 2007.